Vol. 19: 1–13, 2001 | CLIMATE RESEARCH Clim Res | Published November 22

Statistical-dynamical extrapolation of a nested regional climate simulation

Udo Busch*, Dietrich Heimann**

Deutsches Zentrum für Luft- und Raumfahrt (DLR), Institut für Physik der Atmosphäre, 82234 Weßling, Germany

ABSTRACT: A method is introduced by which the results of a regional climate model (RCM) that is temporarily nested in a general circulation model (GCM) are extrapolated in time. The procedure is based on a weather-type classification scheme using cluster analysis. It relies on statistical relationships between GCM and RCM output which are deduced from the overlapping nesting period. For a validation of the extrapolation scheme, a 30 yr GCM simulation of the Hadley Centre with a continuously nested RCM is used. The predictor is the large-scale 500 hPa geopotential height, and the predictands are the regional-scale surface temperature and precipitation. A comparison of the results of the extrapolation scheme with the direct RCM output for the winter temperature and precipitation in Central Europe demonstrates the potential of the method developed. Provided that results of a long-term GCM run are available and the statistics can be transferred from the overlapping period to the extrapolation period, the new method allows a reduction in the computational effort needed for long-term RCM simulations by shortening the integration time considerably.

KEY WORDS: Climate change · Regional climate models · Statistical-dynamical extrapolation · Downscaling

1. INTRODUCTION

Regional climate impact studies require a reliable high-resolution database which describes the regional climate for given scenarios (e.g. von Storch 1995). The regional climate, in turn, is subject to global climate changes and effects of the regional topography. It is a usual procedure to downscale the global-scale climate by nesting a regional climate model (RCM) into a general circulation model (GCM), see, e.g. Giorgi & Mearns (1999) or Takle et al. (1999). The RCM's part is to describe the regional influences on the climate. Therefore the grid spacing has to be fine enough to resolve all topographical features which are relevant to the climate in the region of interest, i.e. the mesh width of RCMs should be on the order of 20 to 50 km (e.g. Stein et al. 2000).

Due to numerical demands, long-term simulations of high-resolution RCMs are extremely expensive in terms of computer time, even if the regional model domain covers only a small fraction of the earth. Therefore, long-term RCM simulations for 10 to 30 yr periods on a 50 km grid (e.g. Jones et al. 1997, Pan et al. 2000) are still quite rare.

It is necessary that the RCM results represent a sufficiently long period in order to average over short-term climate variations. Hence, the RCM runs should extend over the international standard length of a climate period, i.e. 30 yr (WMO 1997). Moreover, it is necessary to consider a possible change in the large-scale climate which could consist of long-term drift of certain parameters (e.g. temperature) and a change in the frequency of occurrence of circulation patterns.

This study presents a new statistical-dynamical method to extend the temporal representativeness of nested RCM runs. It is named the statistical-dynamical extrapolation (SDE) scheme in the following. Provided the results of a long-term GCM simulation are available, the method allows one to limit the simulation time of a nested RCM to a period which is significantly shorter than that of the GCM run. This saves considerable computing time, thus leaving capacity free

*Present address: Deutscher Wetterdienst, Frankfurter Str. 135, 63067 Offenbach, Germany

**Corresponding author. E-mail: d.heimann@dlr.de

for multiple scenario simulations or alternative model assumptions.

Section 2 of the paper describes the methodology. Section 3 deals with the specific application of the method. Results and their validation are discussed in Section 4. Finally, conclusions are drawn in Section 5.

2. METHODOLOGY

2.1. General concept

The new SDE scheme is based on an objective large-scale weather-type classification which resembles the improved statistical-dynamical downscaling method that was introduced by Fuentes (1998) and Fuentes & Heimann (2000).

The GCM time series is divided into a set of successive, non-overlapping multi-day episodes depending on their 500 hPa geopotential height anomaly pattern. The episodes are then classified into weather-type classes according to the spatial patterns and temporal development.

Once each episode is appointed to a class, the frequency of occurrence of each class is determined in the period which is covered by the RCM simulation ('training period') and in the period to which one seeks to extrapolate the RCM results ('prediction period').

Finally, the results of the RCM are class-wise reassembled after weighting them according to the (changed) frequencies of occurrence in the prediction period. The method presumes that the statistical relationships which are found in the training period remain valid in the prediction period.

The application of SDE needs some preparatory measures by which the time series are treated before they are used by the SDE scheme. The preparatory steps are described in Section 2.2, while the core of the method is explained in full detail in Section 2.3.

2.2. Preparation of the time series

Since the purpose of classification is to discriminate episodes with respect to spatial patterns and temporal development, it is necessary to remove both long-term trend and mean annual cycle from the original time series. Different episodes in a class are then comparable regardless the year or month they belong to.

For the necessary preparation of the simulated time series we define:

(1) Temporal mean, $\langle\psi\rangle$:

$$\langle\psi\rangle = \frac{1}{N\cdot K}\sum_{\tau=1}^{N\cdot K}\psi(\tau) \tag{1}$$

(2) Running annual mean, $\overline{\psi}$:

$$\overline{\psi}(\tau) = \frac{1}{N+1}\sum_{\tau=t-N/2}^{t+N/2}\psi(\tau) \quad \text{for } \tfrac{1}{2}N < t < KN-\tfrac{1}{2}N \tag{2}$$

(3) Running monthly mean, ψ^*:

$$\psi^*(t) = \frac{1}{M+1}\sum_{\tau=t-M/2}^{t+M/2}\psi(\tau)-\overline{\psi}(\tau) \quad \text{for } \tfrac{1}{2}M+\tfrac{1}{2}N < t < KN-\tfrac{1}{2}M-\tfrac{1}{2}N \tag{3}$$

(4) Mean annual cycle, $\hat{\psi}$:

$$\hat{\psi}(\tau) = \frac{1}{K}\sum_{i=1}^{K}\psi^*\left(N(i-1)+\tau\right) \quad \text{for } 1 < \tau < N \tag{4}$$

(5) Anomaly, ψ':

$$\psi'(t) = \psi-\left(\overline{\psi}+\hat{\psi}\right) \tag{5}$$

where ψ stands for either 500 hPa geopotential height (H), surface temperature (T) or precipitation rate (P). K is the number of years. N is the number of days per year or season, M is the number of days per month and t denotes the day.

In the following the subscripts 'GCM' and 'RCM' are used to indicate the resolution of the data and their respective source. The subscript 'SDE' marks results of the SDE scheme. The SDE results are in RCM resolution. The superscripts 't', 'p', 'ta', 'pa' and 'f' denote training period, prediction period, alternative training and prediction period (used in Section 4.2) and the full length of the GCM time series, respectively.

2.3. The statistical-dynamical extrapolation scheme

The core of the procedure consists of 4 steps. First, the complete GCM time series is split up into multi-day episodes. Second, similar episodes are grouped in classes. Third, the RCM results of the training period are assigned to the classes and high-resolution mean distributions are calculated for each class. Finally, the regional climate of the prediction period is determined by re-weighting the RCM results of the training period according to the change in the frequency of occurrence of the weather-type classes between training and prediction period.

2.3.1. Determination of multi-day episodes

As a first step towards a classification the large-scale geopotential height anomaly fields $H'^{(f)}_{GCM}$ are divided

into consecutive non-overlapping multi-day episodes. In order to reduce the dimensionality of the problem, $H'^{(f)}_{GCM}$ is approximated by the n leading empirical orthogonal functions (EOFs; see Preisendorfer 1988, Zorita et al. 1995, von Storch & Zwiers 1999) which explain 99% of the variance:

$$H'^{(f)}_{GCM}(i,t) \approx \sum_{k=1}^{n} v_k(t)\,\mathrm{EOF}_k(i) \quad (6)$$

where i is the grid point index, t is the time, EOF_k is the kth EOF, $v_k(t)$ is the amplitude of the pattern at time t and n is the number of EOFs used.

For the division of the whole time series of all winter months (DJF) into multi-day episodes, a hierarchical cluster analysis (e.g. Anderberg 1973, Enke & Spekat 1997) in combination with a spatio-temporal distance measure was applied to the EOFs. The resulting episodes are consecutive and do not overlap. The clustering works such that the variation in the 500 hPa height pattern is rather small within the episodes, but is rather large between neighbouring episodes. Hence, the episodes mirror the persistence of weather. Further details of the procedure are described in Fuentes & Heimann (2000).

2.3.2. Division into classes

To group similar episodes of the same length into classes, a partitioning 'k-means' cluster analysis algorithm was used (Hartigan 1975). The 'k-means' cluster algorithm optimizes a partition of objects into a prescribed number of classes (N_c). The Euclidean distance is used as a measure of similarity. The sum of squared Euclidean distances is minimized within the clusters (classes), whereas it is maximized between the centroids of the different clusters (e.g. Werner & Gerstengarbe 1997). The distance measure always refers to the spatial patterns of the same day in the sequence of the episode and therefore aggregates the episodes also with respect to their temporal evolution. Again we refer to Fuentes & Heimann (2000) for further details.

2.3.3. Extrapolation of the nested regional climate simulations

In opposition to the statistical-dynamical downscaling method of Fuentes & Heimann (2000), the SDE is not based on regional-scale episode simulations but uses the continuous RCM output of the training period in order to predict the regional climate of the prediction period. The only requirements are that the GCM run covers both periods and that all weather-type classes defined in the total GCM period occur in the training period.

To begin with, the regional-scale mean distribution of the anomaly of the predictand ϕ'_{RCM} is class-wise determined from the RCM results of the episodes that belong to the training period. For the kth class it is formed by

$$\langle \phi'_{RCM} \rangle^{(t)}_k = \frac{1}{N^{(t)}_k} \sum_{j=1}^{N^{(t)}_k} \phi'_{RCMj} \quad (7)$$

with $N^{(t)}_k$ being the sum of days which belong to the episodes of class k in the training period.

Now, it is assumed that a regional climatological change of the predictand ϕ can be composed of a change due to a shift in the frequency of large-scale weather types in that region and a general large-scale change which is equally distributed over all weather types (e.g. a generally warmer atmosphere).

Accordingly, an interim extrapolated regional-scale climatology $\tilde{\phi}^{(p)}_{SDE}$ of the prediction period is first determined. It accounts for the effect of a shift in the weather-type frequency. The interim extrapolated regional-scale climatology is generated by weighting the class-specific mean distributions of the training period with the frequencies of occurrence of the classes in the prediction period:

$$\tilde{\phi}^{(p)}_{SDE} = \left(\sum_{k=1}^{N_c} w^{(p)}_k \langle \phi'_{RCM} \rangle^{(t)}_k \right) + \langle \phi_{RCM} \rangle^{(t)} \quad (8)$$

The weights are given by

$$w^{(p)}_k = \frac{N^{(p)}_k}{N \cdot K^{(p)}} \quad (9)$$

with $N^{(p)}_k$ being the sum of days which belong to the episodes of class k in the prediction period. $N \cdot K^{(p)}$ is the total number of days in the prediction period.

As mentioned above, the interim regional-scale climatology already considers the regional climate change due to a changed occurrence of large-scale weather patterns. The circulation types (classes) are associated with characteristic large-scale advection (e.g. cold advection is associated with northerly flow). In addition, the regional topography modifies the large-scale flow, e.g. by foehn effects. These effects are described by the RCM, which considers the topography in high resolution. The interim climatology accounts for large-scale advection and regional topographic effects. It describes the regional climatological distribution of the predictand.

However, the interim extrapolated climatology of ϕ does not include any change which is independent of the frequency of large-scale circulation patterns, e.g. the general warming due to increasing greenhouse gas concentration:

$$\Delta\phi_{GCM}^{(p)-(t)} = \langle\phi_{GCM}\rangle^{(p)} - \langle\phi_{GCM}\rangle^{(t)} \quad (10)$$

This trend of ϕ, if there is any, has to be determined from the GCM output of the full period, i.e. training and prediction period. It is defined as a spatial mean trend in the area which comprises the circulation patterns relevant to the region of interest.

Hence, the desired regional-scale mean of the prediction period, $\langle\phi_{SDE}\rangle^{(p)}$, is the sum of the interim climatology and the large-scale trend:

$$\langle\phi_{SDE}\rangle^{(p)} = \tilde{\phi}_{SDE}^{(p)} + \Delta\phi_{GCM}^{(p)-(t)} \quad (11)$$

At this point it has to be noted that SDE can only consider allochthonous changes of the regional climate, i.e. changes the cause of which is inherent in the large scale and represented by the GCM simulation. SDE fails in predicting regional climate changes of an autochthonous nature. For instance, regional temperature and humidity trends which are due to regional-scale land surface modifications (e.g. irrigation) are beyond the scope of SDE. These modification are included neither in the RCM simulation of the training period nor in the GCM simulation of the total period. However, they can be included in the RCM simulation of the prediction period.

In the following the SDE result $\langle\phi_{SDE}\rangle^{(p)}$ is compared with the simulated regional-scale mean $\langle\phi_{RCM}\rangle^{(p)}$.

3. APPLICATION OF THE METHOD

3.1. Discussion of GCM and RCM output data

The data used to demonstrate and validate the SDE scheme were generated by the GCM HadAM2 and the RCM HadRM2 of the UK Met Office Hadley Centre. HadAM2 and HadRM2 are hydrostatic primitive equation models employing regular longitude-latitude grids of a resolution of 3.75° × 2.5° (approx. 275 km) and 0.44° × 0.44° (approx. 50 km), respectively. Both models comprise 19 levels, defined on a hybrid vertical coordinate. The HadAM2 (GCM) is a global model and the HadRM2 (RCM) covers the eastern Atlantic and whole Europe. The time steps of GCM and RCM are 30 and 5 min, respectively. Model results were made available as daily mean values or daily extremes. Detailed information of the model physics is given by Jones et al. (1995).

A study of Noguer et al. (1998) describes a transient climate experiment with the HadAM2 and HadRM2 that is comparable to the one used here. It considers the radiative impact of increasing greenhouse-gas concentrations represented by an equivalent atmospheric CO_2 increase of 1% yr^{-1} and the direct effect of increasing concentration of sulphate aerosols. This corresponds approximately to IPCC scenario IS92a (IPCC 1996).

The GCM integration starts in the year 1990. The overlapping period of the GCM and the nested RCM lasts from 2006 to 2035, i.e. a period of 30 yr. It is the longest available time series of a nested RCM for this region.

The original idea was to use the pair of 30 yr time series provided by the GCM and nested RCM to demonstrate that, with the help of the new SDE scheme, the regional climatology of the full 30 yr period can be reproduced by only a 10 yr subset of RCM results without unacceptable loss in quality. Because for June, July and August of the model year 2017 all GCM and RCM data were lost and could not be recovered (R. Jones pers. comm. 2000), it was first decided to restrict the study to the winter season, i.e. December, January and February (DJF). Then a closer inspection of the winter data revealed some inconsistencies between GCM and RCM results which would adulterate the statistical relationships between the 2 scales and thus impedes the SDE method. Inconsistencies between driving GCMs and nested RCMs are a general problem in long-term nested model simulations (see von Storch et al. 2000). Fig. 1 shows that the monthly mean temperatures as simulated by GCM and RCM deviate by more than 5 K in the months December 2016 and January 2030 (arrows). These months are consequently excluded from further utilization. Another reason for dropping these months is the fact that the simulated (GCM) monthly mean temperatures are so low (–6.9°C in December 2016 and –6.8°C in January 2030) that, assuming a Gaussian standard distribution, they correspond to events of a 250 yr return rate.

Eventually, two 10 yr periods (DJF only) were selected as training and prediction period, namely 2007/08–2016/17 (without December 2016) and 2017/18–2026/27.

3.2. Setup

In the actual application we take the anomaly patterns of the 500 hPa geopotential height as the large-scale predictor. The spatial domain of the 500 hPa geopotential height data extends over 33.75° W–26.25° E and 35–65° N. This area is presented in Fig. 2. The large-scale predictor is provided by the GCM simulation.

The hierarchical cluster analysis (Section 2.3.1) was applied in a way that the GCM time series was subdivided into episodes of 2, 3, 4 and 5 d length. This range of days is centred around the peak period in the atmospheric energy spectrum over Central Europe (3 to 4 d). The number of classes prescribed in the k-means

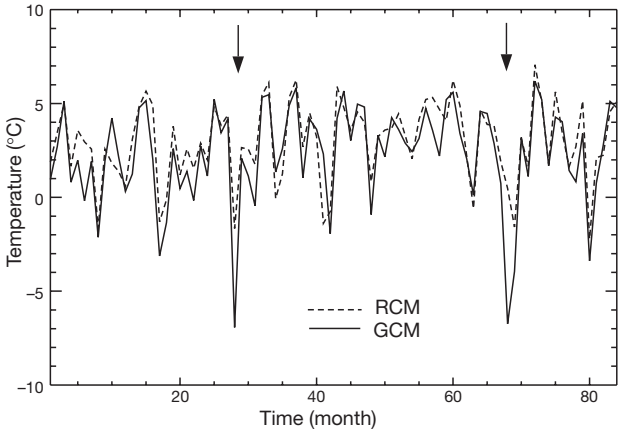

Fig. 1. Time series of the simulated monthly mean 1.5 m temperature averaged over Central Europe in the winter months (DJF) from December 2007 to February 2035. Arrows point to deviations of >5 K

cluster analyses scheme (Section 2.3.2) was chosen as follows: 2 classes for the 2 d episodes, 5 classes for the 3 d episodes, 10 classes for the 4 d episodes and 5 classes for the 5 d episodes, i.e. altogether $N_c = 22$ classes. This choice ensures that the number of elements in each class does not vary too much.

The 22 classes are summarized in Appendix 1. Fig. A1 shows the centroids (temporal mean) of the geopotential height anomaly for all classes. Table A1 lists the classes, describes their type, and provides their frequencies in either period.

The SDE is used to predict the average 1.5 m temperature and precipitation in the prediction period. The application focusses on the greater Alpine Region. This area comprises 24 × 18 grid points of the RCM domain, i.e. approx. 1200 × 900 km^2 (the inner frame in Fig. 2). The Alps exert a significant influence on the regional climate in central Europe. It is expected that the fine-mesh (50 km resolution) RCM considers this influence to a certain degree, at least in a much better way than the coarse-grid (275 km resolution) GCM.

4. RESULTS AND VALIDATION

4.1. Temperature

Before the benefit of the SDE method is discussed, the effect of resolution (GCM vs RCM) is demonstrated with the help of the simulated mean winter temperature in the training period (2007/08–2016/17). Fig. 3a clearly illustrates the ability of the nested fine-mesh RCM to simulate detailed and topographically induced spatial structures. For instance, the influences of the Alps and the Adriatic and Mediterranean Sea cause specific signatures in the mean temperature field. On the contrary, the coarse-grid GCM (Fig. 2a) is not able to simulate these details, because the topography cannot be sufficiently resolved. Analogously, the simulated change of the mean winter temperature from the training period (2007/08–2016/17) to the prediction period (2017/18–2026/27) shows remarkable differences. The GCM predicts a considerable warming of up to 2 K in the winter months. This warming is concentrated in central and western Europe and Scandinavia (Fig. 2b). However, the 275 km resolution pre-

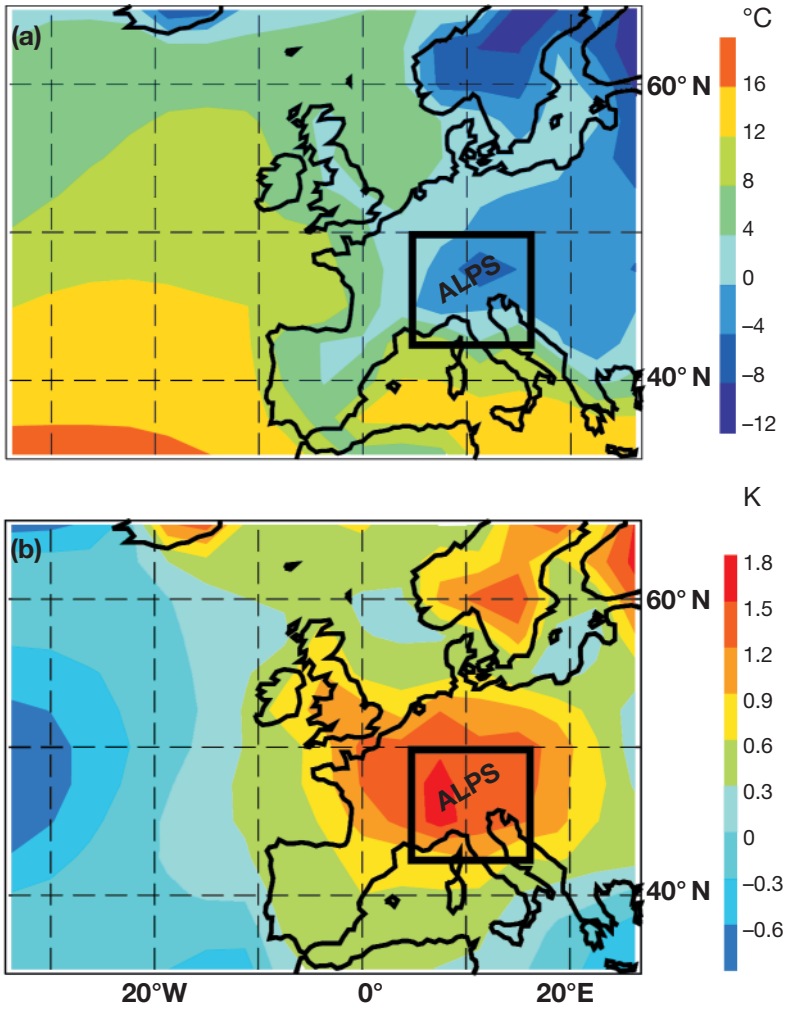

Fig. 2. Results of the GCM: (a) mean winter temperature of the training period, $T^{(t)}_{GCM}$, (b) change of the mean winter temperature from the training period to the prediction period, $\Delta T^{(p)-(t)}_{GCM}$

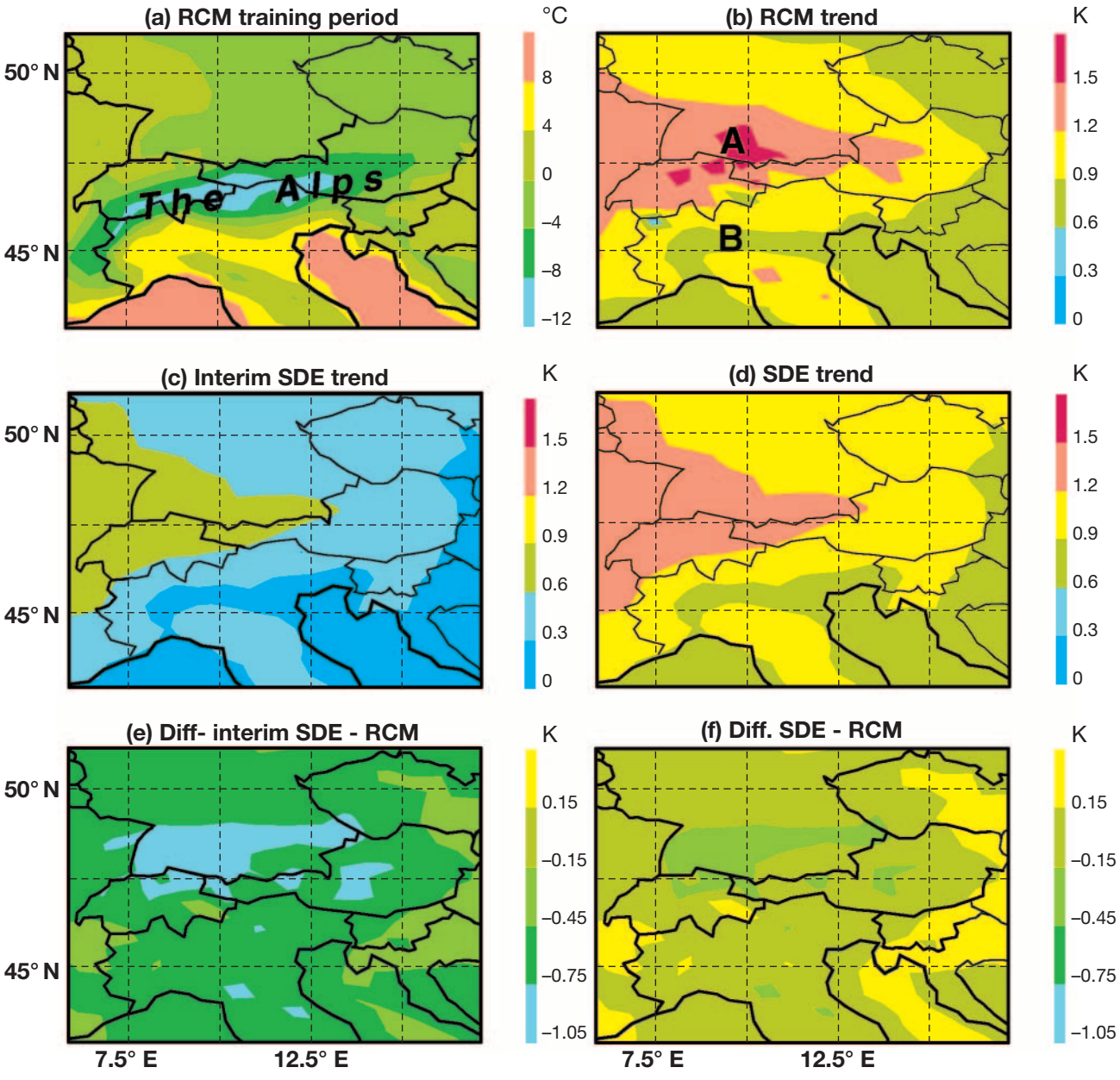

Fig. 3. Results of RCM and SDE: (a) RCM mean winter temperature of the training period, $T^{(t)}_{RCM}$, (b) RCM change of the mean winter temperature, $\Delta T^{(p)-(t)}_{RCM}$ (A and B indicate locations referred to in Section 4.1 and Fig. 4), (c) interim SDE change of the mean winter temperature, $\tilde{T}^{(p)}_{SDE} - \langle T_{RCM}\rangle^{(t)}$, (d) SDE change of the mean winter temperature, $\tilde{T}^{(p)}_{SDE} - \langle T_{RCM}\rangle^{(t)}$, (e) difference between interim SDE change and simulated RCM change, $\tilde{T}^{(p)}_{SDE} - \langle T_{RCM}\rangle^{(p)}$, and (f) difference between SDE change and simulated RCM change, $T^{(p)}_{SDE} - \langle T_{RCM}\rangle^{(p)}$

vents the GCM from capturing the influence of the Alpine topography in a realistic way. The nested RCM with 50 km resolution apparently modifies the GCM trend in the vicinity of the Alps (Fig. 3b). The increase in the mean temperature is generally lower in the RCM run. The maximum warming is less intensive (only 1.6 K instead of 1.9 K) and shifted to the northern rim of the Alps. In the Po valley south of the Alps the warming is considerably lower (0.6 to 0.9 K) than predicted by the GCM (1.5 to 1.8 K). The spatial structures in the RCM temperature-change field are not visible in the GCM simulation. The only coincidence of both model simulations is the gradual weakening of the warming from west to east.

In the following it is assumed that, because of its higher resolution, the RCM is more precise and reliable than the GCM. However, the gain in accuracy and reliability takes place to the debt of the compu-

tational efficiency. It is now a question of whether the SDE method is able to predict the temperature change between the 2 periods with the same quality but without having the prediction period explicitly simulated with the RCM. The answer is provided by Fig. 3c and d. They show the interim SDE change, $\tilde{T}_{SDE}^{(p)} - \langle T_{RCM}\rangle^{(t)}$, and the final SDE change, $\langle T_{SDE}\rangle^{(p)} - \langle T_{RCM}\rangle^{(t)}$, respectively. The interim field demonstrates that the main spatial patterns of the temperature change are due to the frequency shift in large-scale weather types between the training and prediction periods. The altered frequencies of weather types apparently led to a relative warming north of the Alps and a corresponding cooling south of them. The reason for this is probably the decrease in frequency of weather types with northerly flow (Types 7, 13 and 17; see Appendix 1) and the corresponding increase in westerly and southerly flow situations (Types 10 and 12; see Appendix 1). Northerly flow advects cool polar air and often leads to blocking and orographically enhanced cloudiness and precipitation along the northern rim of the Alps. This, in turn, gives rise to relatively low temperatures. If these types of flow become less frequent, the mean temperature will rise. Moreover, an increase in southerly to westerly flow types strengthens the advection of warm Mediterranean air and invokes additional foehn effects north of the Alps, thus leading to additional warming.

After adding the spatially averaged GCM temperature change between the 2 periods, $\Delta T_{GCM}^{(p)-(t)} = 0.62$ K (see Eq. 10), the quantitative agreement between SDE prediction and RCM prediction is almost perfect (compare Fig. 3d with Fig. 3b).

The basic features of the regional temperature change are well captured and the spatial correlation of SDE and RCM temperature change reaches up to 0.99. The deviations between SDE and RCM are in the range ±0.3 K. The average absolute error amounts to only 0.13 K. This deviation has to be assessed relative to the amount of warming between the 2 periods, which is 1.1 K on average. Hence, the relative error is only 12%. As compared to the bias of regional climate simulations with respect to observations (locally more than 2 K, Nouger et al. 1998, Takle et al. 1999), the deviation of the SDE prediction from the RCM simulation is acceptable.

So far, the results were discussed with respect to mean temperature values. However, the SDE method is also able to predict frequency distributions und thus the probability of temperature values being in excess of defined thresholds. In Fig. 4 fitted theoretical frequency distributions (standard distribution including skewness and kurtosis) are shown for 2 selected locations within the RCM domain: Lake Constance ('A' in Fig. 3b) and Po valley ('B' in Fig. 3b), where the RCM predicts the maximum and minimum warming, respectively. At both locations the RCM simulates a shift towards higher temperatures and a decrease in variance. At Lake Constance the frequency of cold temperatures (–10 to –5°C) decreases substantially. If, as a first guess, the large-scale GCM temperature change is added to the RCM result of the training period, only a minor shift of the frequency distribution to higher temperatures is achieved. Hence, the major part of the predicted change is attributed to the alteration of weather-type frequencies or autochthonous changes. The results show that SDE improves the first guess, but cannot fully predict the simulated distributions. While the result in the Po valley is acceptable, the decrease in cold events at Lake Constance could not be sufficiently predicted. Moreover, an increase in warm

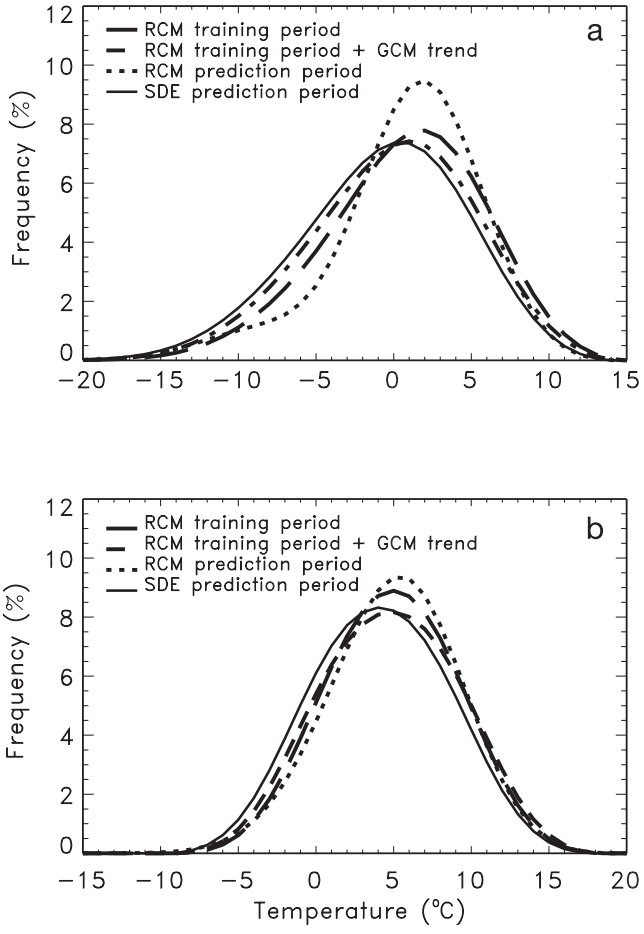

Fig. 4. Fitted theoretical frequency distributions of the 1.5 m temperature with respect to 1 K intervals in the winter months (upper panel: Lake Constance – 'A' in Fig. 3b; lower panel: Po valley – 'B' in Fig. 3b)

events (>10°C) was predicted by SDE but does not occur in the RCM results.

4.2. Precipitation

Due to its high spatial and temporal variability, the numerical simulation of precipitation is known to be crucial. Nevertheless, the attempt was made to apply the SDE method to the mean winter precipitation rate in the greater Alpine region. In contrast to temperature, no GCM precipitation data are available. Therefore, the step from the interim SDE climate $\tilde{P}^{(p)}_{SDE}$ to the final SDE climate $P^{(p)}_{SDE}$ was omitted. Consequently, $P^{(p)}_{SDE} = \tilde{P}^{(p)}_{SDE}$, i.e. the change predicted by SDE only, reflects the change in the frequency of occurrence of large-scale weather types. Fig. 5 presents the corresponding results.

The explicitly simulated mean winter preciptiation rate in the training period ($P^{(t)}_{RCM}$; Fig. 5a) shows the largest values along both sides of the Alpine main crest. The simulated patterns are similar to those observed in the present climate (Frei & Schär 1998).

The RCM calculates a rather heterogeneous field of precipitation change from the training period to the prediction period ($\Delta P^{(p)-(t)}_{RCM} = \langle P_{RCM}\rangle^{(p)} - \langle P_{RCM}\rangle^{(t)}$; Fig. 5b). In most parts of the region, the mean precipitation rate is predicted to change merely in the range ± 0.3 mm d^{-1}. Only in the Po valley south of the Alps does the precipitation rate decrease by more than 0.3 mm d^{-1}. The simulated regional change in precipitation is apparently not consistent with the frequency change in large-scale weather types (see Appendix 1). From a decreasing frequency of northerly flow and a contemporarily increasing frequency of southerly flow, one would actually expect a reduction of precipitation north of the Alps and an amplification south of it. This is apparently not the case. Therefore it is not surprising that the simulated change $\Delta P^{(p)-(t)}_{RCM}$ could not be reproduced by the SDE method ($\Delta P^{(p)-(t)}_{SDE} = P^{(p)}_{SDE} - \langle P_{RCM}\rangle^{(t)}$; Fig. 5d). The patterns of RCM and SDE results differ substantially. The spatial

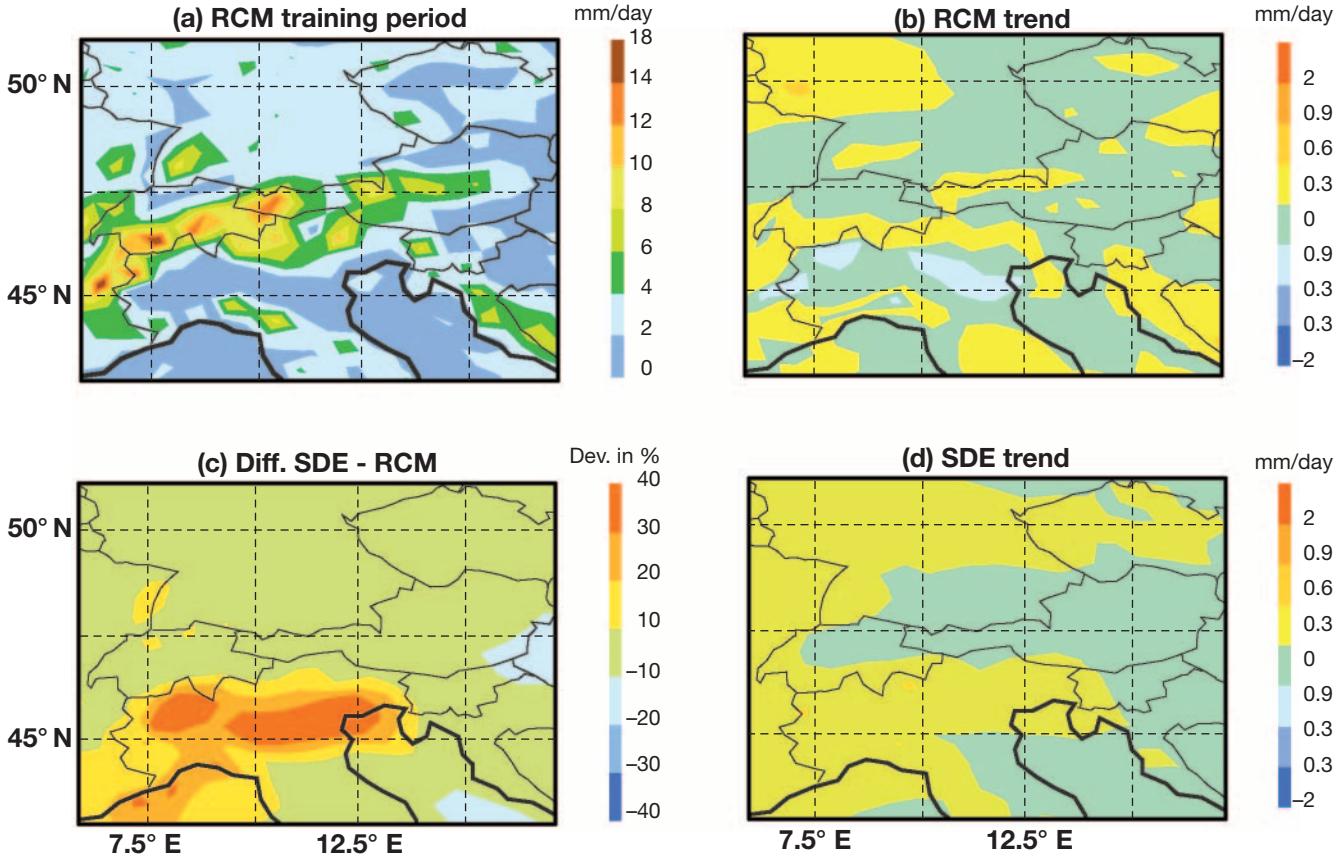

Fig. 5. Results of RCM and SDE: (a) RCM mean winter precipitation rate of the training period, $P^{(t)}_{RCM}$, (b) RCM change of the mean winter precipitation rate, $\Delta P^{(p)-(t)}_{RCM}$, (c) difference between SDE change and simulated RCM change, $P^{(p)}_{SDE} - \langle P_{RCM}\rangle^{(p)}$, (d) SDE change of the mean winter precipitation rate $P^{(p)}_{SDE} - \langle P_{RCM}\rangle^{(t)}$

correlation coefficient amounts to only +0.1. Nevertheless, the SDE result deviates from the RCM result by only ±10% in most parts of the region. Particularly strong differences of more than 40% occur in the Po valley, where the results even disagree in sign. The result also shows that, in contrast to temperature, the addition of a horizontally averaged large-scale change to the interim SDE climate would not lead to an improvement.

There are 2 possible reasons for the failure of SDE: (1) the change from the training period to the prediction period is statistically insignificant, i.e. the predicted change is by and large of random nature; (2) the statistical relationships between GCM and RCM found in the training period are no longer valid in the succeeding prediction period, for example, because of autochthonous changes of climatologically relevant regional processes.

In order to prove which reason is more likely, we checked the statistical significance of the simulated change. In addition, we redefined training and prediction periods such that they are representative of the same climatic state. This was done by selecting every other winter of the 20 yr period 2007/08–2026/27 as the training ensemble $P^{(ta)}_{GCM}$ and the remaining winters of the same 20 yr period as the prediction ensemble $P^{(pa)}_{GCM}$.

If the change from one to the other period is not significant, SDE will not be able to predict it. On the other hand, the prediction of the alternating winters should be successful in the case of reason (2). This is due to the fact that the same climate is considered in both ensembles, e.g. any climate drift from one to the other ensemble is excluded.

The results of the alternative SDE application are presented in Fig. 6 and the significance criterion is given in Fig. 7. The results suggest that both reasons apply. The change from the training period to the prediction period $\Delta P^{(p)-(t)}_{RCM}$ is not significant in most parts of the domain, except south of the Alps, where the 90% level of significance is exceeded (Fig. 7a). In the Po valley even the 95% level of significance was reached.

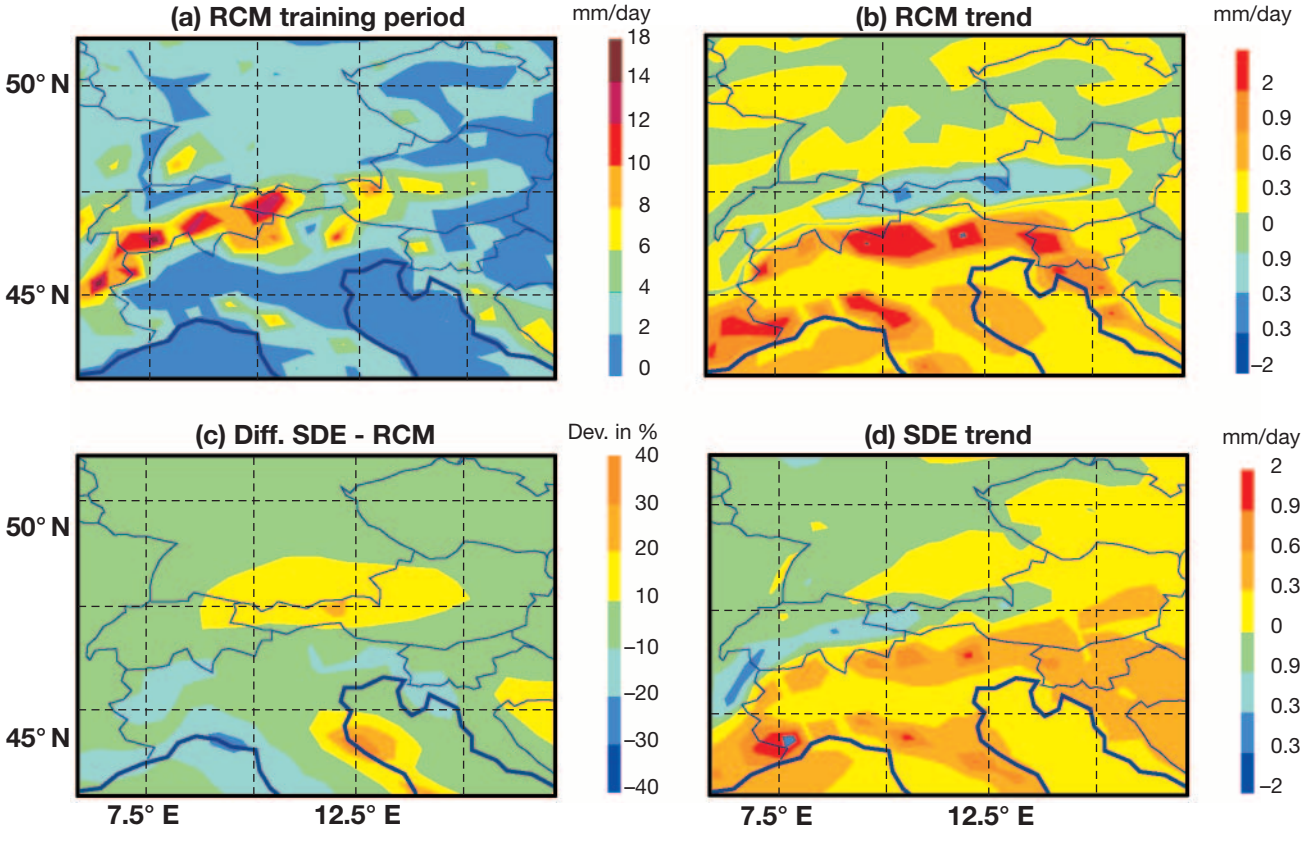

Fig. 6. Results of RCM and SDE for merged periods: (a) RCM mean winter precipitation rate of the training period, $P^{(ta)}_{RCM}$, (b) RCM change of the mean winter precipitation rate, $\Delta P^{(p)-(ta)}_{RCM}$, (c) difference between SDE change and simulated RCM change, $P^{(pa)}_{SDE} - \langle P_{RCM} \rangle^{(pa)}$, (d) SDE change of the mean winter precipitation rate, $P^{(pa)}_{SDE} - \langle P_{RCM} \rangle^{(ta)}$

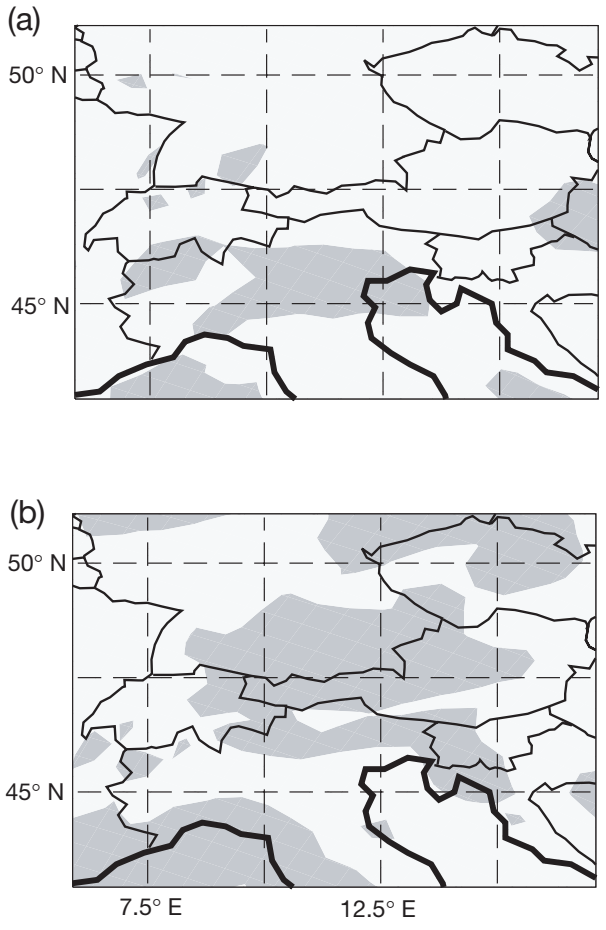

Fig. 7. Shaded areas indicate where the RCM predictions of the mean precipitation rate are significant with respect to the 90% significance level: (a) change from training to prediction period $\Delta P^{(p)-(t)}_{RCM}$, (b) change between periods with alternating winters $\Delta P^{(pa)-(ta)}_{RCM}$

However, the SDE prediction $\Delta P^{(p)-(t)}_{SDE}$ also fails in this area. On the other hand, the application of SDE to the alternating winter ensembles turned out to be rather successful. Training and prediction ensembles differ from each other in the precipitation rate at the northern and southern foot of the Alps ($\Delta P^{(pa)-(ta)}_{RCM}$; Fig. 6b). This change is statistically significant, as Fig. 7b shows. The spatial structure of the mean precipitation change between the 2 ensembles is fairly well reproduced by the SDE method ($\Delta P^{(pa)-(ta)}_{SDE}$; Fig. 6d). However, the amplitude of the SDE change is slightly too weak. A similar result is obtained if the training and prediction ensembles are exchanged.

In summary, SDE did not only fail in all areas where the simulated change is not significant. South of the Alps, where the change was actually proved to be significant, SDE even failed in sign. As a straightforward interpretation, it follows that the simulated increase in precipitation south of the Alps is not caused by an increased frequency of weather-types conducive to high precipitation (e.g. southerly flow with blocking and orographic lifting). It seems to be much more the case that some weather-types produce more precipitation in a changed climate, possibly because of increased evaporation over the Mediterranean Sea. However, it is beyond the scope of this paper to discuss the reasons for this. It is also not the intention of this study to speculate on the reasons for a biannual oscillation in the simulated precipitation, which might have caused the significant difference between the ensembles of alternating winters. Nevertheless, it can be stated that SDE was able to predict the change in precipitation when climatologically relevant drifts were excluded.

5. CONCLUSIONS

The SDE scheme allows the extension of the temporal validity of nested RCM simulations to a longer period provided the longer period is simulated by the driving GCM. The SDE method yields regional mean parameters with the same spatial resolution and approximately the same accuracy as they would be provided by a continuously nested RCM run. The benefit of SDE is a considerable reduction in the computational requirements.

An extrapolation of the mean winter temperature from one decade to the next in a transient climate-change experiment shows the promising ability of the method developed. Even secondary features of the regional temperature change between the 2 decades are fairly well reproduced. A comparison of the SDE results with the direct RCM output shows a spatial correlation of 0.99 and a mean absolute temperature deviation of merely 0.13 K. In addition, the frequency distribution of temperature values in the prediction period could be estimated by SDE. However, the uncertainty is larger as in the case of the mean value.

The unsuccessful application of SDE to precipitation revealed some restrictions. SDE cannot reproduce statistically insignificant changes because they are not determined by large-scale changes. They are much more random results which reflect the internal variability. In addition, it was shown that robust statistics between GCM and RCM which describe the allochthonous part of regional-scale changes are a necessary prerequisite for the application of SDE. The statistics are impaired by autochthonous contributions to the regional climate changes. SDE was able to predict precipitation changes which were not influenced by the latter.

The influence of the length of the prediction and training periods was not tested in this study. Furthermore, no studies have been carried out to optimize the SDE scheme, for instance, by using additional large-scale predictands such as humidity. This will be addressed in future work.

Acknowledgements. The development of our method was strongly stimulated by Prof. Bennert Machenhauer during the definition phase of the European MERCURE project. The data of the HadAM2 (AGCM) and the HadRM2 (RCM) simulations were kindly provided by the Hadley Centre for Climate Research of the UK Meteorological Office. Our special thanks go to Dr Richard Jones, who made the data available. In particular, we would like to thank Dr David Hassell and Dr Kate Ward for their assistance in copying the data from the archives of the Hadley Centre. Financial support was provided by the European Commission through grant ENV4-CT97-0485 and by the Bundesministerium für Bildung und Forschung (BMBF) through grant 07DLR06/0.

Appendix 1. Properties of the 22 classes resulting from the k-means cluster analyses

The SDE method takes the anomaly patterns of the 500 hPa geopotential height as the large-scale predictor. The spatial domain of the large-scale data used is 33.75° W–26.25° E and 35–65° N. Fig. A1 shows the centroids of the derived 22 clusters, i.e. the arithmetic mean of the 500 hPa geopotential height anomalies $\langle H'_{GCM} \rangle_k^{(f)}$ of all episodes within each weather-type class k.

In Table A1 the resulting circulation patterns are subjectively associated with the well-established 'Großwetterlagen' after Hess & Brezowsky (see Gerstengarbe et al. 1993). The frequency change from the training to the prediction period is indicated. In general, the frequency of westerly and southerly weather types increases and that of northwesterly and northerly weather types decreases. Furthermore, the weather type with high pressure over central Europe becomes less frequent while the weather types with high pressure over the Norwegian Sea and Fenno-Scandinavia become more frequent.

Table A1. Frequency of occurrence (in %) of the 22 weather-type classes in the training period and in the prediction period and the sign of the frequency change from the training period to the prediction period. The weather-type specifications correspond with the 'Großwetterlagen' after Hess & Brezowsky (see text). The separation of the 2, 3, 4 and 5 d classes is emphasized with horizontal lines

Class	Weather type	Training period (%)	Prediction period (%)	Sign of frequency change
1	Cyclonic west weather condition	3	4	+
2	Anticyclonic northerly weather condition	4	3	–
3	Anticyclonic northeasterly weather condition	4	3	–
4	Cyclonic northwesterly weather condition	8	5	–
5	Trough central Europe	5	6	+
6	Anticyclonic southerly weather condition	3	6	+
7	Cyclonic northerly weather condition	5	3	–
8	Trough west Europe	6	4	–
9	Anticyclonic northeasterly weather condition	4	4	
10	Cyclonic west weather condition	7	13	+
11	High pressure area over Fennoscandinavia	3	9	+
12	Cyclonic southerly weather condition	7	9	+
13	Cyclonic northerly weather condition	6	5	–
14	Anticyclonic southeasterly weather condition	2	2	
15	High pressure area central Europe	8	2	–
16	Cyclonic northwest weather condition	5	3	–
17	High pressure area British Island	3	2	–
18	Anticyclonic southerly weather condition	3	3	
19	Cyclonic southerly weather condition	6	4	–
20	Anticyclonic west weather condition	3	4	+
21	Cyclonic northerly weather condition	2	2	
22	Trough central Europe	3	4	+

Appendix 1 (continued)

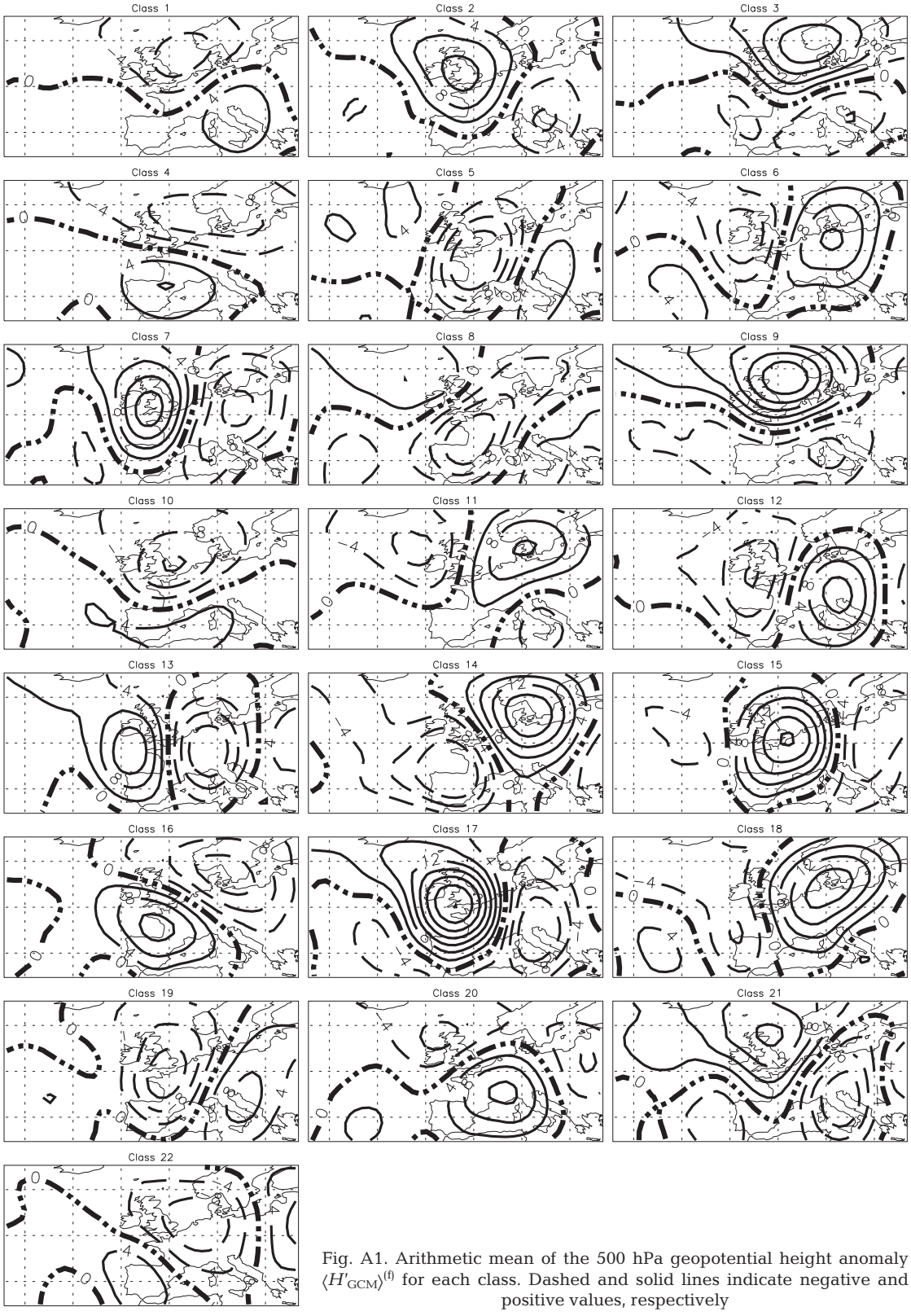

Fig. A1. Arithmetic mean of the 500 hPa geopotential height anomaly $\langle H'_{GCM} \rangle^{(f)}$ for each class. Dashed and solid lines indicate negative and positive values, respectively

LITERATURE CITED

Anderberg MR (1973) Cluster analysis for applications. Academic Press, New York

Enke W, Spekat A (1997) Downscaling climate model outputs into local and regional weather elements by classification and regression. Clim Res 8:195–207

Frei C, Schär C (1998) A precipitation climatology of the Alps from high-resolution rain-gauge observations. Int J Climatol 18:873–900

Fuentes U (1998) Statistical-dynamical downscaling based on a classification of synoptic weather types and their evolution. PhD thesis, Meteorological Institute, University of Munich

Fuentes U, Heimann D (2000) An improved statistical-dynamical downscaling scheme and its application to the Alpine precipitation climatology. Theor Appl Climatol 65: 119–135

Gerstengarbe FW, Werner PC, Busold W, Rüge U, Wegener KO (1993) Katalog der Großwetterlagen Europas, nach Paul Hess und Helmut Bresowsky 1881–1992. 4. Auflage. Ber Dtsch Wetterdienst 113

Giorgi F, Mearns LO (1999) Introduction to special section: regional climate model revisited. J Geophys Res 104: 6335–6352

Hartigan J (1975) Clustering algorithms. Wiley, New York

IPCC (1996) Climate change 1995 — the science of climate change. Houghton JT, Meira-Filho LG, Callander BA, Harris N, Kattenberg A, Maskell K (eds). Cambridge University Press, Cambridge

Jones RG, Murphy JM, Noguer M (1995) Simulation of climate change over Europe using a nested regional-climate model. I: Assessment of control climate, including sensitivity to location of lateral boundaries. Q J R Meteorol Soc 121:1413–1449

Jones RG, Murphy JM, Noguer M, Keen AB (1997) Simulation of climate change over Europe using a nested regional-climate model. II: Comparision of driving and regional model responces to a doubling of carbon dioxide. Q J R Meteorol Soc 123:265–292

Noguer M, Jones RG, Murphy JM (1998) Sources of systematic errors in the climatology of a nested Regional Climate Model (RCM) over Europe. Clim Dyn 14:691–712

Pan Z, Christensen JH, Arrit RW, Gutowski WJ Jr, Takle ES (2000) Ten-year U.S. regional climate simulations for impact assessments. In: 11th Symposium on Global Change Studies. Long Beach, CA, 9–14 January 2000, American Meteorological Society, Boston

Preisendorfer RW (1988) Principle component analysis in meteorology. Elsevier, Seattle

Stein J, Richard E, Lafore JP, Pinty JP, Asencio N, Cosma S (2000) High-resolution non-hydrostatic simulations of flash-flood episodes with grid-nesting and ice-phase parametrization. Meteorol Atmos Phys 72:203–221

Takle ES, Gutowski WJ Jr, Arritt RW, Pan Z and 16 others (1999) Project to intercompare regional climate simulations (PIRCS): description and initial results. J Geophys Res 104:19443–19461

von Storch H (1995) Inconsistencies at the interface of climate impact studies and global climate research. Meteorol Z NF 4:72–80

von Storch H, Zwiers FW (1999) Statistical analysis in climate research. Cambridge University Press, Cambridge

von Storch H, Langenberg H, Feser F (2000) A spectral nudging technique for dynamical downscaling purposes. Mon Weather Rev 128:3664–3673

Werner PC, Gerstengarbe FW (1997) Proposal for the development of climate scenarios. Clim Res 8:171–182

WMO (1997) Climatological normals (CLINO) for the period 1961–1990, WMO No. 847. World Meteorological Organization, Geneva

Zorita E, Hughes JP, Lettenmaier DP, von Storch H (1995) Stochastic characterization of regional circulation patterns for climate model diagnosis and estimation of local precipitation. J Clim 8:1023–1042

Editorial responsibility: Hans von Storch, Geesthacht, Germany

Submitted: July 13, 2000; Accepted: December 12, 2000
Proofs received from author(s): September 13, 2001